# A NOVEL FACILITY FOR TESTING AT LOW REYNOLDS NUMBER

**Ernest S. Hanff***

***Institute for Aerospace Research, National Research Council of Canada**

**Keywords**: *MAV, glycerine, vicous test medium*

## Abstract

*The advent of advanced flow control methods using MEMS and micro-blowing or suction, as well as the development of micro aerial vehicles (MAV) has significantly increased interest in low Reynolds number flows. Aerodynamic testing in this regime using conventional facilities, such as wind or water tunnels, is seriously hampered by the necessary small model sizes and low testing speeds, rendering it very difficult to diagnose the flow with adequate spatial resolution and to measure aerodynamic loads with sufficient accuracy. In order to address these limitations, a novel proof-of-concept pilot facility specifically intended for low Reynolds number testing has been built and is described. It is based on the use of a high kinematic viscosity test medium, which allows testing super-scale models at the correct Reynolds number. Given the usefulness of the particle image velocimetry (PIV) technique, correction methods were developed to allow its use in this environment, where the optics move with the model, and tracking errors are unavoidable.*

## 1 Introduction

In the recent past there have been considerable advances in various enabling technologies such as nanotechnology, functional materials, smart structures, electronic miniaturization, sensors, systems integration, artificial intelligence, etc. which are facilitating the development of micro aerial vehicles (MAV) with practical characteristics. By virtue of their unobtrusiveness, from a military standpoint, these vehicles can be valuable tools for information gathering in the local combat arena, including urban settings, as well as in anti-terrorism activities. Depending on the on-board sensors, optical, acoustic, chemical, biological and radiation information can be obtained. Clearly the versatility of MAV also makes them attractive for use in non-military applications such as drug and contraband interdiction, hazardous accident site inspections involving chemical, biological and nuclear releases and numerous other applications. Due to their small size and low speeds, MAV operate in a very low Reynolds number flow regime shown, together with those corresponding to various other flight vehicles, in Fig. 1 [1].

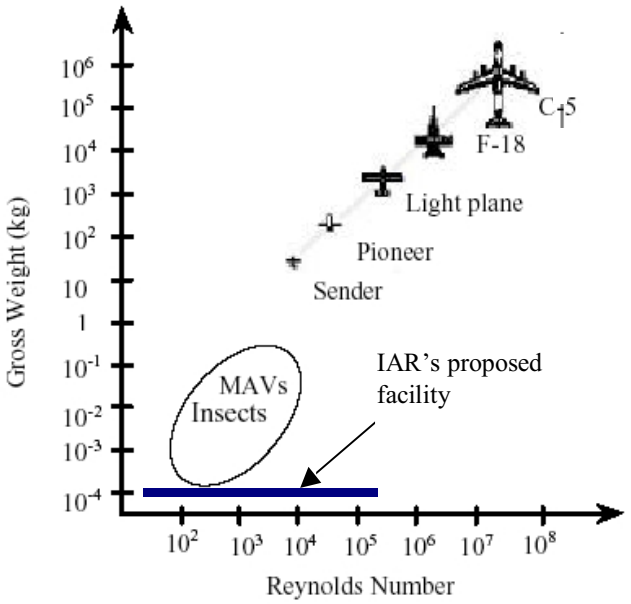


Fig. 1 Reynolds number regime for various flight vehicles [1]

The requirement to better understand low Reynolds number aerodynamics, particularly unsteady aerodynamics, is not only driven by the advent of MAV but also by the development of advanced flow control systems based on MEMS, micro blowing and suction. Finally, from a theoretical point of view, there is a need to better understand boundary layer behavior, particularly with regards to transition, partly in order to develop improved numerical predictions.

Some of the limitations in our understanding of the above flows stem from a lack of facilities capable of providing high quality experimental data under the conditions at hand. It is known that conventional facilities, such as wind or water tunnels, are not suitable when operating under these conditions because, in order to simulate the required Reynolds number, the model size and test velocity must be very small. This results in two main problems: poor spatial resolution of flow diagnostics due to the very small size of the flow features of interest, and insufficient measurement accuracy of the very small generated aerodynamic loads.

Clearly, in the case of MAV development, it is imperative to have high-quality experimental data in order to develop the highly efficient aerodynamic designs required to achieve practical performance characteristics in spite of these vehicles' extremely limited ability to carry the necessary propulsion energy sources. Furthermore, high-quality data is also required to correctly validate CFD codes that can then be used to support the development of these vehicles. Likewise, in the case of flow control methods, a clear understanding of the underlying physics promotes the development of more efficient and effective methods.

A feasibility study on a novel concept for low Reynolds number testing was undertaken that culminated with the construction of a pilot facility which is the subject of the present paper. Although, the facility was mainly built to prove the proposed concept, it is also being used to conduct limited tests. Samples of experimental results are also presented. Knowledge gained from the use of the pilot facility is being incorporated into the design, currently under way, of a full-scale research/production facility.

## 2 Facility Principle

The problems associated with conventional test facilities operating in the low Reynolds number regime can be addressed by using a test medium having a kinematic viscosity higher than that of air, such that experiments may be conducted on super-scale models. Eq. 1 shows that to test at a given Reynolds number, the higher the kinematic viscosity, the larger the model can be for a given test velocity and the higher the velocity can be for a given model size.

$$\mathrm{Re} = \frac{V\ell}{\nu} \qquad (1)$$

where Re: Reynolds number, $V$ : velocity, $\ell$ : model reference length and $\nu$: kinematic viscosity of the fluid

Various liquids have a high kinematic viscosity and satisfy the necessary Newtonian characteristics. However glycerine (glycerol) was chosen because it is physiologically innocuous, is clear for flow visualization purposes and is soluble in water in any concentration. Drawbacks are its relatively high cost and strong hygroscopic properties. A comprehensive set of physical properties of glycerine may be found in [2].

By changing the concentration of an aqueous solution of glycerine it is possible to vary its kinematic viscosity continuously by three orders of magnitude, from that of pure water to that of pure glycerine as depicted in Fig. 2. The kinematic viscosity of air corresponds approximately to that of a 2/3 solution of glycerine. Utilizing the complete range of glycerine concentration, and speeds up to the maximum of 1 m/s, it is possible to test a typical model with a 30 cm reference length over an unprecedented range of $25 < \mathrm{Re} < 250{,}000$, which not only covers the laminar and transitional flow regimes, but overlaps with test

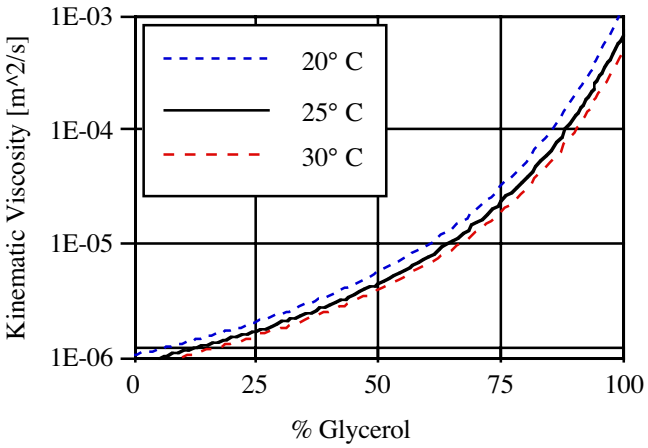


Fig.2 Glycerine solution kinematic viscosity

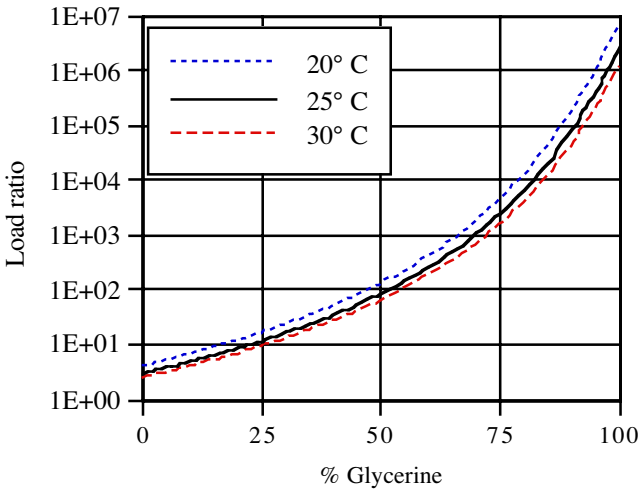


Fig. 3 Load ratio in glycerine solution and air

conditions achievable with conventional facilities. The Reynolds number operational range of the facility is shown in Fig. 1.

The increased allowable model size and test velocity in conjunction with the high test-fluid density compared to that of air, leads to a very important increase in the generated aerodynamic loads at an arbitrary Reynolds number. It can be shown that for a given Reynolds number, the forces acting on the model of a given configuration are independent of model size and are given by [3] :

$$F_x = k\rho v^2$$

where $k$ is a constant and $\rho$ is the fluid density.

Based on the above expression, the ratio of forces acting on a model immersed in a glycerine solution to those acting on it in air for a given Reynolds number are depicted in Fig. 3, which demonstrates the dramatic increase in the loads that can be obtained through the use of this type of test medium. It can be seen that for a given Re, the loads in water are a modest three times those encountered in air, while in pure glycerine they are over a million times higher than in air. Interestingly, for a 2/3 solution of glycerine ($\nu \cong \nu_{air}$), the loads are approximately a thousand times those in air.

Control of the test medium viscosity has the important benefit of increasing the testing flexibility by introducing an additional degree of freedom to the test conditions. Such flexibility is particularly relevant in dynamic experiments where the simulation of angular rates (or frequencies) is important and where the actual rates (frequencies) may be limited by practical considerations.

## 3 Facility Implementation

Rather than forcing the test medium through the facility such as in a wind or water tunnel, which under low Reynolds number conditions leads to problems due to the rapid boundary layer growth on the test section velocity profile, an approach akin to a towing tank, where the fluid is stationary and the model is moved through it, has been used. However, the free surface present in towing tanks, also known to introduce problems, has been eliminated by adding a roof featuring a slot with an appropriate seal at the centerline. All air is eliminated by filling the tank right up to the seal, thus preventing the formation of a free surface. Access to the tank is possible at one end of the facility where the roof can be opened and where a mechanism for the insertion and removal of the model is provided.

General views of the pilot facility are shown in Fig. 4 and Fig. 5. The tank has a cross-section of 1m x 1m and the test section, featuring glass floor and windows, is 3 m long. The access section, which has metal floor and walls, is 1.2 m long. A roof with a longitudinal slot at the centerline of the tank covers the test section. The roof is slightly sloped up towards the center in order to allow the escape of air bubbles through the slot. The vertical sides of the latter

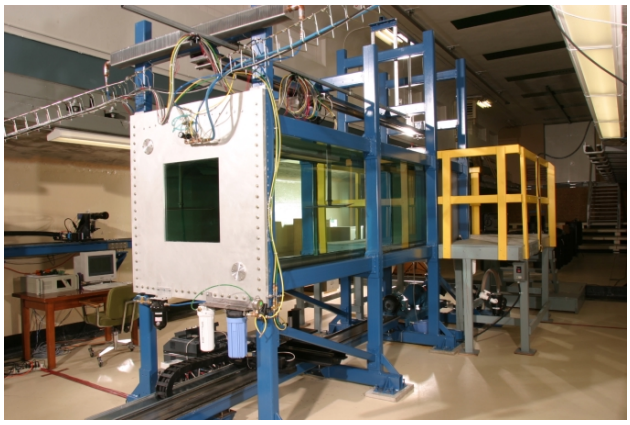

Fig. 4 General view of the facility

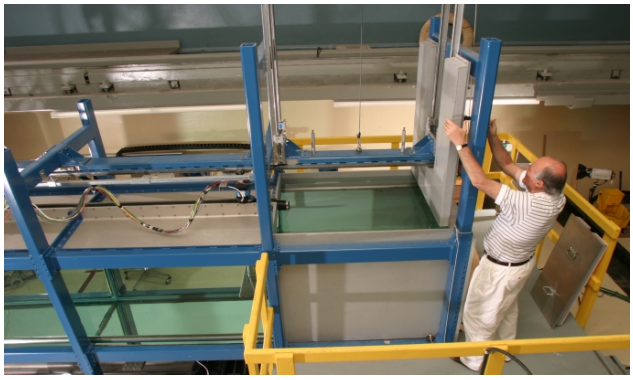

Fig. 5 Top view of pilot facility

support a pair of inflatable rubber seals facing each other, which make contact when inflated, sealing the slot, yet allowing the passage of the model support strut. The tank is filled with the test medium up to and slightly above the line of contact between the opposing seals, which ensures the absence of a free surface and provides lubrication between the seal and the model support strut. The top end of this strut is mounted on a motorized carriage that travels along longitudinal precision tracks located above the tank, thus imparting the needed motion to the model. Tightly controlled arbitrary motions can be imparted to the model, which is important to investigate transient phenomena such as those resulting from impulsive starts and stops, as well as to modulate the forward velocity in response to changes in drag and thrust as encountered in flapping wing flight.

Insertion and removal of the model is accomplished by opening the access section lid, and moving the model carriage to the exposed area. A lifting mechanism is then used to raise or lower the corresponding part of the model carriage track, Access to the model as well as tare measurements are possible when the model is in its raised position (Fig. 5).

A pair of cylindrical manifolds, featuring orifices facing towards the tank center, are located at two diagonally opposite corners of the tank and connected to an external pump. They are used to circulate the test medium, required to remove contaminants through filtration, to create sufficient fluid motion inside the tank to lift off seeding material that settles on the bottom, as well as to disperse persistent dye traces when using a very viscous test medium. Use of the pilot facility has shown that it is necessary to have one rotating manifold in each corner to better carry out some of these functions, a feature that has been incorporated in the design of the full-scale facility.

## 4 Testing Capabilities

Most conventional aerodynamic testing techniques can be used in the facility. In order to perform flow visualization, additional tracks, parallel to the one supporting the model carriage, are installed under and to one side of the tank (Fig.4). The motion of the model carriage and those of carriages mounted on these tracks are controlled by a multi-channel motion control system to ensure that they move in synchronism. Flow visualization experiments are conducted by mounting cameras on the external carriages to record the behavior of dyes released upstream of, or from appropriate ports on the model. Examples of visualization of the flow around a schematic flapping wing model during the downstroke are shown in Fig. 6 for two radically different Reynolds numbers. Fig. 6 (a) obtained in glycerine at Re = 10 (based on forward velocity) and a reduced frequency $\Omega$= 5, and Fig. 6 (b) obtained in water at Re = 8.000

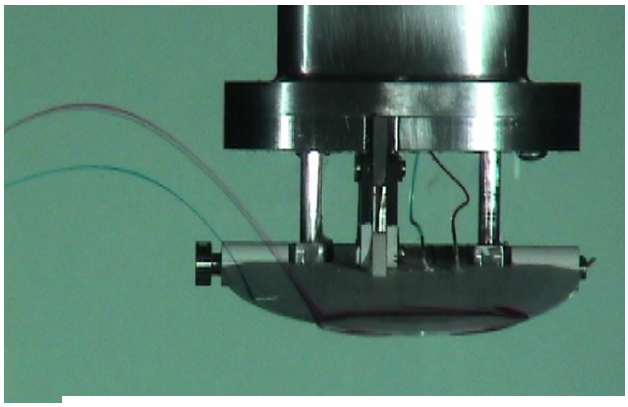

(a) Re=10, Ω=5 in glycerine

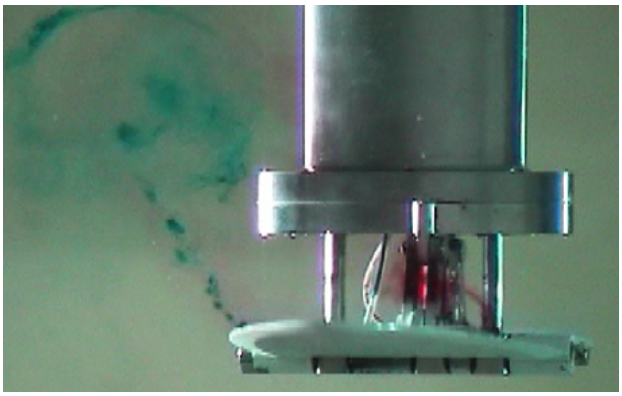

(b) Re=8000, Ω=6.7 in water

Fig. 6 Flow visualization of flapping wing during downstroke

and Ω = 6.7, show the effect of Reynolds number on the flow. At the very low value the flow is fully attached while at the higher value separation occurs, resulting in the wrapping of the shear layers into leading and trailing edge vortices.

Accurate force and moment measurements may be obtained by virtue of the large loads resulting from the high viscosity test medium, allowing the use of conventional balance designs. Provision must of course be made to avoid electrical problems by coating the balance with materials that are impervious to both water and glycerine.

## 5 PIV Measurements

PIV tests are typically conducted by mounting the laser unit on the bottom carriage and the camera on the side one, although the opposite arrangement can also be used. Implementing the PIV technique in this type of facility poses special problems, because the model and optical equipment, rather than being stationary as is the case in wind or water tunnel applications, must all move in synchronism. In spite of the fact that the carriages are mounted on precision tracks and linear bearings and are reasonably accurately controlled by servomotors, there are residual motion errors.

Three possible sources of error are possible: 1) Mis-tracking between the laser sheet and the model , 2) mis-tracking between the camera and the model, and 3) undesired variations in the speed of the model. These errors and methods to correct them, when necessary, are discussed below.

*1) Mis-tracking between the laser sheet and the model*

When the laser light sheet is in a longitudinal plane, as is typically the case, the tracking error between the model and the laser unit clearly has no deleterious effect. If there is a transversal component in the laser sheet orientation, the error results in a very small motion (with respect to the model) of the illuminated volume, which in the vast majority of case is negligible and does not require correction.

*2) Mis-tracking between the camera field of view and the model*

In this case the situation is quite different. Keeping in mind that any jitter of the camera field of view results in a direct spurious velocity error corresponding to the relative motion of that field with respect to the model within one frame pair, it is clear that this effect cannot be ignored. In fact it has been found that velocity errors of up to 50% can be present due to this phenomenon. The motions of the carriages are reasonably accurate (to within 0.07 mm from the ideal position based on the servomotors encoder error signals) and tests conducted with an accelerometer mounted on the camera carriage showed maximum speed variations of about 5%, suggesting that the camera carriage

velocity jitter is insufficient to account for the totality of the observed velocity field errors.

It is therefore likely that angular motions of the camera induced by small vibrations of its carriage account for an important part of the error. Such angular motions cause significant displacements in the field of view due to the magnifying effect of the long distance (>3m) between the camera and the subject plane. Consequently, in order to mitigate the jitter problem, two changes will be implemented in the final facility namely, the camera track will be installed next to the tank, and a higher accuracy rack and pinion system will be used to provide a smoother carriage motion. It is unlikely however that these measures will suffice to completely eliminate the errors, so it will still be necessary to correct them by using appropriate procedures.

*3) Undesirable variations in model velocity*

Just like the camera carrier is subjected to speed variations, so is the model one. As is discussed later, this phenomenon is unimportant as far as mean velocity values is concerned but it has a very significant effect on RMS quantities.

## 5.1 Correction Methods

First the correction for error 2) above is considered. Inasmuch as this error is introduced by the motion of the camera field of view with respect to the model, it is necessary to determine the displacement of the former with respect to the latter that occurs between the two frames in a PIV pair. This is accomplished by using markers on the model, whose positions in both frames provide the necessary information.

In the general case, where the field of view is assumed to translate vertically and horizontally as well as to rotate about the camera optical axis, two markers are required to correct for the above motion. Specifically, if we assume that a Cartesian coordinate system (X,Y) is associated with the camera image, the error due to the motion of the field of view with respect to the model will cause any point (x,y) in the first frame to appear as (x', y') in the second frame, given by

$$\begin{aligned} x' &= (x - x_0)\cdot\cos\theta + (y - y_0)\cdot\sin\theta \\ y' &= (y - y_0)\cdot\cos\theta - (x - x_0)\cdot\sin\theta \end{aligned} \qquad (2)$$

where $x_0$ and $y_0$ are the translation components and $\theta$ is the rotation of the field of view between the two frames[1]. The locations of both markers in the two frames are used to determine these parameters as follows:

Let the coordinates of markers 1 and 2 be given in the first frame by $(x_1,y_1)$, $(x_2,y_2)$ and in the second frame by $(x_1',y_1')$, $(x_2',y_2')$, in which case

$$\theta = \tan^{-1}\frac{y_2 - y_1}{x_2 - x_1} - \tan^{-1}\frac{y_2' - y_1'}{x_2' - x_1'} \qquad (3)$$

Solving (2) leads to the coordinate system displacements

$$\begin{aligned} x_0 &= x_1 - x_1'\cdot\cos\theta + y_1'\cdot\sin\theta \\ y_0 &= y_1 - y_1'\cdot\cos\theta - x_1'\cdot\sin\theta \end{aligned} \qquad (4)$$

Here $x_0$ and $y_0$ are expressed in terms of the coordinates of marker 1 only. The same equations can be used with marker 2. Although mathematically both approaches lead to the same values, in practice there may be small differences, suggesting the use of the average of the two solutions.

Once the displacements and rotation angle of the field of view with respect to the model are known, two equivalent methods can be used to obtain the corrected velocity field:

a) A vector field can be calculated that corrects for the error when added to the velocity vector field obtained using the original two images, and

b) One image can be shifted such that its marker positions are made to coincide with those in the other image, thus eliminating the error, and performing the PIV calculations on these images

[1] This discussion only refers to the error component of the field of view motion. The correct motion, corresponding to the freestream velocity, yields the desired velocity field information and is not considered here.

Method a)

The two components of the displacement due to mistracking at any given point (x,y) between the two images are:

$$\Delta x = x - x' \quad \text{and} \quad \Delta y = y - y' \qquad (5)$$

where the prime coordinates are given by Eqns. 2.

Eqns.5 define the components of the correcting vector field that need to be added to the velocity field obtained using the original two images. An example of such a field is given in Fig. 7 where an exaggerated displacement of the markers is used for the sake of clarity.

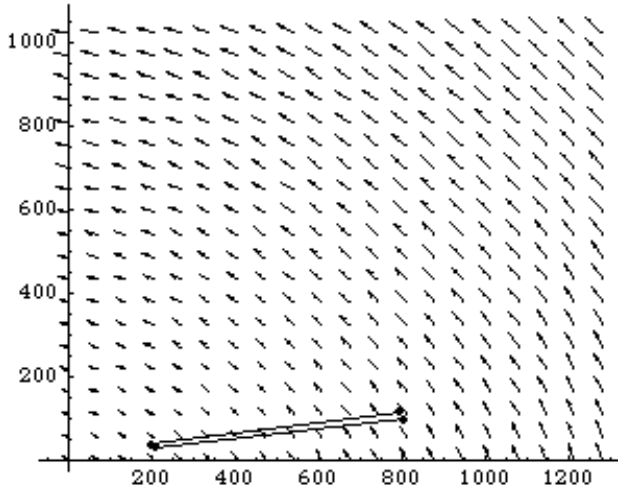


Fig. 7 Tracking error vector correcting field

Method b)

Equations (5) also correspond to the amount by which every point on one image must be shifted in order to compensate for the error due to jitter.

To maintain sub-pixel accuracy, a method was implemented that causes the intensity centroid of each pixel in the original image to be placed at the correct location on the shifted image. This is accomplished by appropriately "smearing" the shifted pixel into adjacent locations ascribing to each an intensity that results in their combined centroid being at the desired location. To preserve the intensity information, the sum of the intensity count of the pixels generated above is made equal to the corresponding value of the original pixel. Although three pixels are sufficient to perform the above operation, it was found that the computational process is expedited by using the four pixels surrounding the desired centroid location. The intensity at each of these pixels is given in terms of the original unshifted pixel intensity ($I_0$) by:

$$I(y_c^-, x_c^-) = (y_c^+ - y_c)(x_c^+ - x_c) I_0$$
$$I(y_c^-, x_c^+) = (y_c^+ - y_c)(x_c - x_c^-) I_0$$
$$I(y_c^+, x_c^-) = (y_c - y_c^-)(x_c^+ - x_c) I_0$$
$$I(y_c^+, x_c^+) = (y_c - y_c^-)(x_c - x_c^-) I_0$$

where $x_c$ and $y_c$ are the coordinates of the centroid and superscripts - and + denote truncated integer value and the next higher integer respectively.

Examples of the intensity distribution needed to obtain the stipulated centroid locations are shown in Fig. 8 for $I_0$=1000. Finally, the intensity at any pixel in the shifted image is simply the sum of the values contributed by applying the above process to all the pixels on the original image.

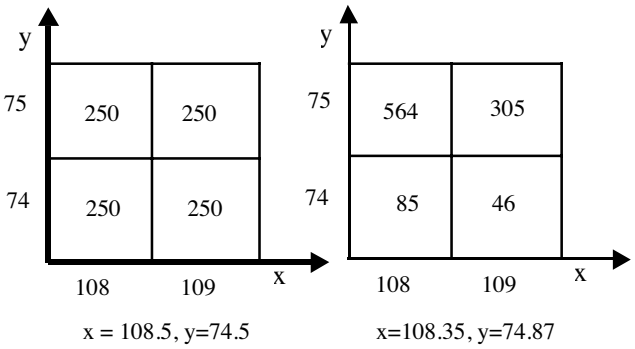


Fig. 8 Pixel centroid location

Inasmuch as methods a) and b) are equivalent, it is to be expected that the corrected velocity field obtained with them are the same. In fact no significant differences were found between the results obtained using the two correction approaches. Not only does the image shifting method obviate the need for larger interrogation windows (or shorter $\Delta t$) in the presence of large jitters, but as is shown below, it has the added advantage of facilitating the measurement of statistical flow quantities. Given that PIV software packages derive these quantities from

the local velocity at fixed locations (referenced to the camera field of view) in a multiplicity of velocity fields, the motion of the model (between frame pairs) relative to this field causes errors, particularly in the immediate vicinity of the model. Specifically, it becomes necessary to replicate a situation where the model remains stationary with respect to the camera.

In order to accomplish this, one frame is selected as a reference for a run or series of runs under the same test conditions. All other frames are shifted such that their markers coincide with the reference one, which automatically fulfills both the requirement for intra and inter frame pairs jitter correction.

If the above corrections are carried out, the mean flow properties are suitably obtained, however RMS quantities such as turbulence intensity are significantly overestimated. This has been ascertained by comparing these values under quiescent conditions, where all carriages are stationary, with those present under testing conditions. In the far field, particularly upstream of the model, there should be a close agreement between them, which is not the case. The explanation lies in the fact that the above corrections are intended to compensate for the relative motion of the camera field with respect to the model. If the model motion is slightly uneven due to jitter (error *3)* previous section) , so will that of the corrected camera field of view be with respect to the test fluid, resulting in slight observed velocity errors that significantly affect RMS quantities. The problem can be reduced by having a better control of the carriages velocities which is going to be implemented in the full-scale facility. A temporary software "fix" is being developed which consists of adding a correcting vector field to each velocity field such that the instantaneous velocity in two appropriately selected small regions in the far field correspond to the average value for the run (or sets of runs under given test conditions) in those locations. Clearly, this forces the RMS values in those locations to be null, however the errors over the whole frame are expected to be reduced.

## 5.2 Application of correction method

PIV measurements, described in the next section, were made on a wing model mounted upside down to observe the flow over its top surface by means of a vertically oriented streamwise laser sheet. The camera was located outboard of the model, with its height and orientation adjusted such that the intersection between the light sheet and model surface could just be discerned. In these tests the markers were implemented by means of four light emitting diodes (LEDs) mounted on a fixture placed inside the hollow model which can thus be seen by the camera. To minimize camera lens chromatic aberration problems, green LEDs with a wavelength within a few nanometers from that of the laser, are used. The LEDs are covered by masks with a small orifice sized to produce a suitable image size (~10 pixels in diameter). Additional size control can be achieved by varying the LED light intensity. The fixture is shown in Fig. 9, where one of the LED masks is not installed. Focusing of the markers is accomplished by adjusting the spanwise position of the fixture within the model cavity so that it is in the same plane as the laser sheet.

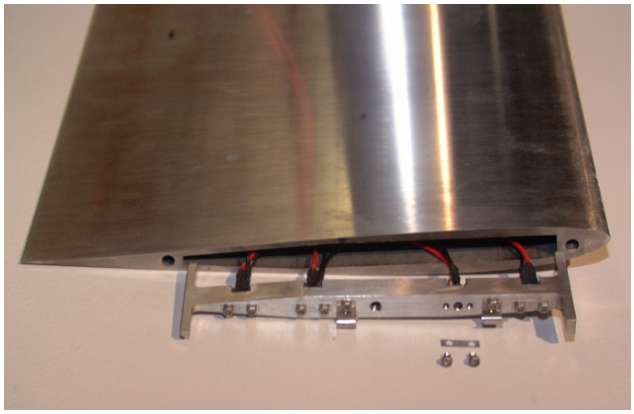

Fig.9 LED markers fixture (1 mask removed)

In order to obtain a well defined model location, the markers are turned on for approximately 3 microseconds in synchronism with the two laser

flashes. LED drive currents many times larger than the rated ones are required to obtain sufficient light intensity to suitably record the marker images, which proved to be possible by virtue of the very small LED duty cycle (~1/1000).

To determine the coordinates of the two markers, which for accuracy considerations should be as far apart as possible, two small rectangular windows centered at the nominal marker locations (obtained by inspection on one image in a set of runs) are defined. The shape of these windows is such that they are fully within the dark area in the model cavity, where the only source of light is one marker, and are sufficiently large to accommodate the maximum marker displacements due to tracking errors. Low background light readings are eliminated by forcing the intensity levels below an arbitrary threshold value to be zero.

In order to determine a marker coordinate with sub-pixel accuracy, the "center" of the marker is obtained by: applying the following equations to all pixels in the window

$$\bar{x} = \frac{\sum_i x_i \cdot f(I_i)}{\sum_i f(I_i)} \quad \text{and} \quad \bar{y} = \frac{\sum_i y_i \cdot f(I_i)}{\sum_i f(I_i)}$$

where *f(I)* is an arbitrary monotonically increasing function of the local intensity count. It has been found that *f(I) = I*, which leads to the intensity centroid, provides good results. This simple algorithm does not assume any specific intensity distribution, which is not a limitation as it is used to locate the relative position of the same marker, with similar distribution, in two frames. The correction methods have been implemented using off-line processing. In order to accelerate the processing of large numbers of frames, the code is being rewritten and integrated with the PIV software.

### 5.3 Experimental Results

Tests were conducted to investigate the flow over a 3.62 aspect ratio wing with a Selig SD7003 low Reynolds number profile. Views of the model above the facility access section and during testing are shown in Fig. 10and Fig. 11 respectively.

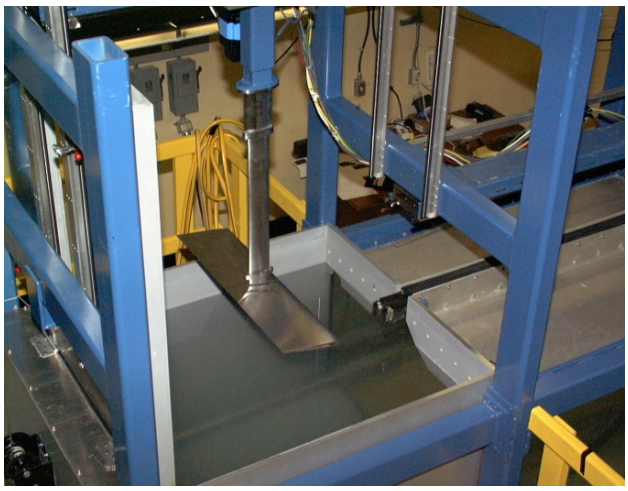

Fig. 10 Model above facility access section

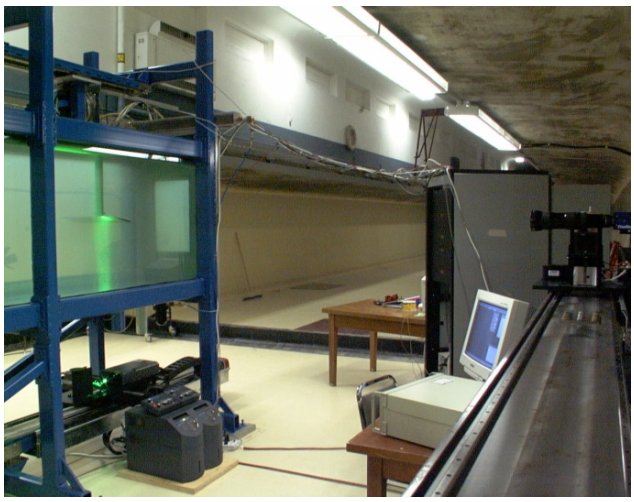

Fig. 11 Model in test section for PIV test

The flow was seeded with 20 microns polyamid particles chosen for their specific gravity of 1.03, which results in an extremely low settling speed in water. A 300mm lens was used to provide the spatial resolution required to obtain the desired data. The flow field at two thirds span was selected for the investigation. At that location the width of the field of view is 75 mm

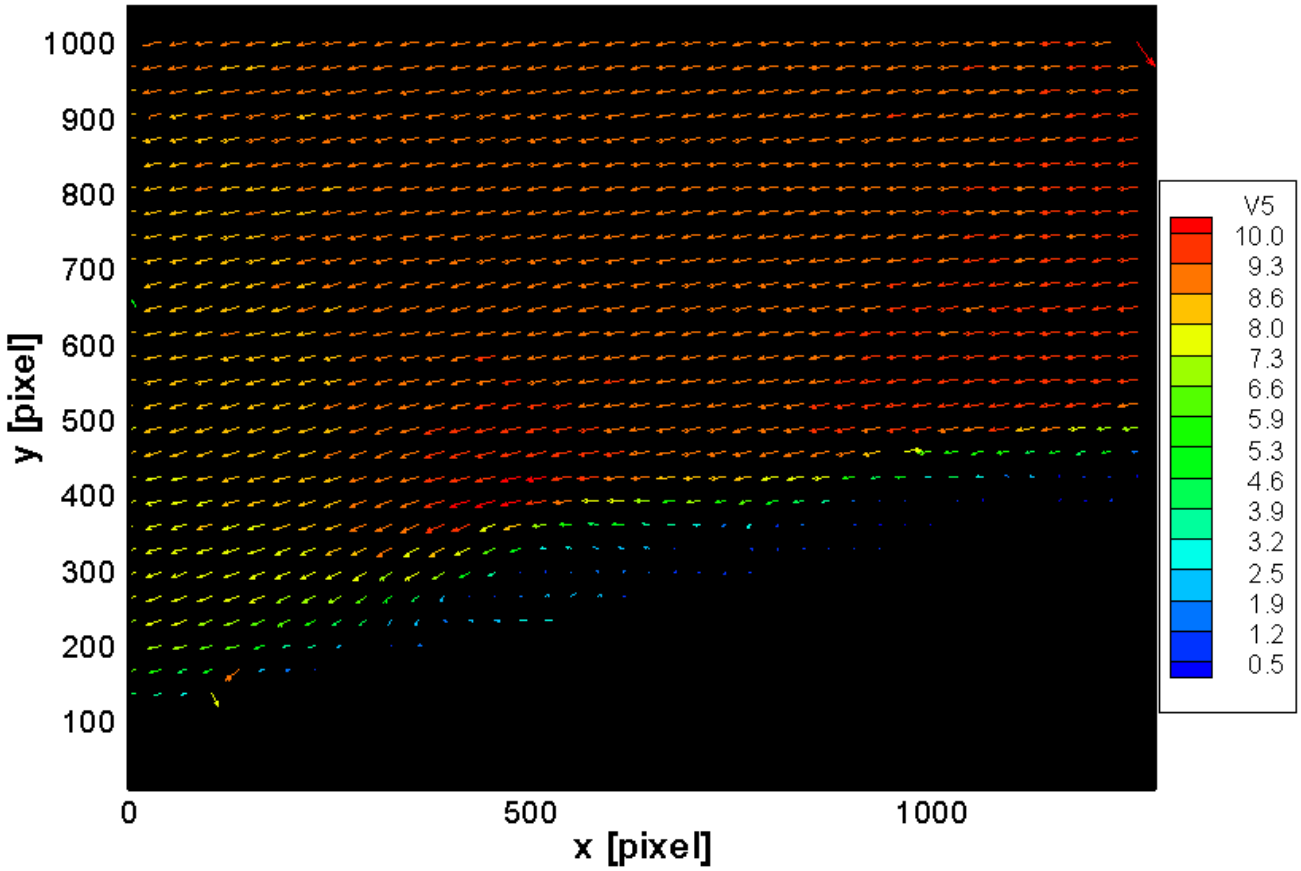


Fig. 12 Instantaneous velocity field

corresponding to 37% of the model chord. Hence, images of the flow field at three different chordwise locations were used to obtain the flow over most of the wing.

A typical instantaneous velocity field over the aft part of the model at an angle of attack of 6.5° and a Reynolds number of 20,000 is shown in Fig.12 where the model has been masked out and flow is from right to left.

The field was obtained using three passes with interrogation windows of 32x32 pixels and 50% overlap. In this case a "roller" shed from the laminar separation bubble located further forward on the wing has been captured. The velocity legend is given in pixel displacements, where freestream velocity corresponds to 8 pixels.

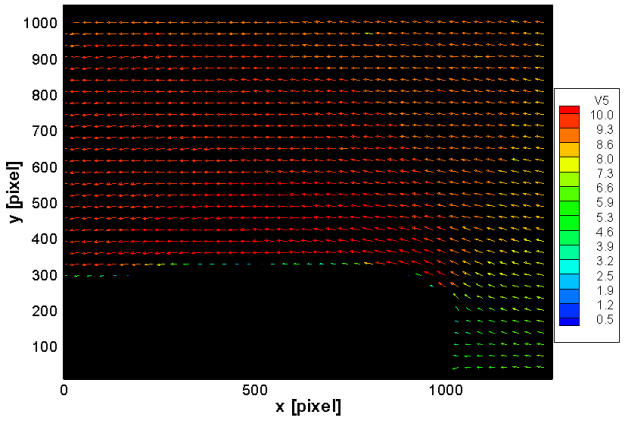


Fig. 13 Mean velocity field

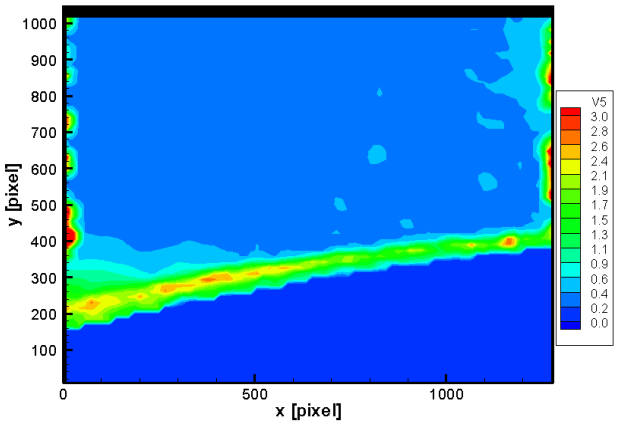


Fig. 14 $|u'_{RMS}+v'_{RMS}|$ over central section

The mean velocity field over the forward part of the wing for $\alpha$=7° and Re=60k is shown in Fig. 13 whereas Fig. 14 depicts a contour plot of $|u'_{RMS}+v'_{RMS}|$ over the central part of the wing for $\alpha$=7° and Re=40k. As already mentioned, the minimum value of close to 1 pixel in the latter figure is significantly over estimated due to the uncorrected error caused by the non-ideal motion of the model. The high values near the vertical edges are artifacts caused by the lateral image shifts needed to move the markers of all frames to the same location on the frames.

## 6 Conclusions

A pilot facility, based on a novel concept specifically intended for aerodynamic testing at low Reynolds numbers, has been built and used to conduct preliminary flow visualization and PIV experiments. Correction methods, needed to account for tracking errors introduced by the unconventional requirements for PIV testing in this environment have been developed and validated. Use of the pilot facility has demonstrated the value of the concept and has suggested improvements that are being incorporated into the design of a full-scale research/production one.

## 7 Acknowledgements

The financial support of AFRL and the contribution of Dr. Michael Ol from that organization towards the implementation of the PIV technique in the pilot facility are gratefully acknowledged.

## 8 References

[1] McMichael J M, Francis M S. Micro Air Vehicles - Toward a New Dimension in Flight, www.darpa.mil/tto/MAV/mav_auvsi.html, 1997.

[2] Dow Chemical, Physical Properties of Glycerine, http://www.dow.com/glycerine/resources/physicalprop.htm

[3] Hanff E. Advanced low Reynolds number testing facility, *Proc. 18th UAV Systems International Conf.*, Bristol, April, paper 27, 2003.